Materials Science & Engineering A 688 (2017) 210–217

Contents lists available at ScienceDirect

Materials Science & Engineering A

journal homepage: www.elsevier.com/locate/msea

Processing of ultrafine-grained titanium with high strength and good ductility by a combination of multiple forging and rolling

Z. Bézi[a], G. Krállics[b,*], M. El-Tahawy[c,d], P. Pekker[e], J. Gubicza[c]

[a] Department of Structural Integrity and Production Technologies, Engineering Division, Bay Zoltán Nonprofit Ltd., H-3519 Miskolc, Hungary
[b] Institute of Physical Metallurgy, Metalforming and Nanotechnology, University of Miskolc, H-3515 Miskolc-Egyetemváros, Hungary
[c] Department of Materials Physics, Eötvös Loránd University, H-1117 Budapest, Hungary
[d] Department of Physics, Faculty of Science, Tanta University, 31527 Tanta, Egypt
[e] MTA-ME Materials Science Research Group, H-3515 Miskolc-Egyetemváros, Hungary

ARTICLE INFO

Keywords:
Grade 2 titanium
Multiple forging
Rolling
UFG microstructure
Strength
Ductility

ABSTRACT

The microstructure and the mechanical properties of Grade 2 titanium semi-products processed by a combination of multiple-forging and subsequent plane rolling are studied. It is shown that the application of this technology on Grade 2 titanium doubled the strength without considerable deterioration of ductility at room temperature. The high strength is caused by the ultrafine-grained (UFG) microstructure with high dislocation density. The minimum grain size and the maximum dislocation density achieved by the combined method were very low (~560 nm) and high (~18×10^{14} m^{-2}), respectively. Mechanical modelling suggests that the effectiveness of multiple forging in grain refinement is mainly caused by the large, homogeneous imposed strain in non-monotonic strain path, similar to conventional severe plastic deformation (SPD) methods. The total equivalent strain at the end of the rolling step is about 4.4. The good ductility of this material can be attributed to the coarse grains embedded in the UFG matrix which formed due to dynamic recovery and recrystallization at the elevated temperature of rolling. It is proved that the combined method of multiple-forging and plane rolling might be a candidate technology in mass-production of UFG titanium with improved mechanical properties.

1. Introduction

Severe plastic deformation (SPD) techniques can be effectively used for the increase of strength in metallic materials. The hardening in SPD-processed materials is achieved mainly by the strong grain refinement as pointed out in the review paper prepared by Langdon [1]. However, Gubicza et al. [2] showed that the large dislocation density formed during SPD has also a significant effect on the yield strength. Estrin and Vinogradov [3] revealed that the consecutive application of SPD methods may yield a finer grain size and a higher strength, as compared to individual procedures. Equal channel angular pressing (ECAP) is often used as an individual SPD technique [4] or as a processing step in combined SPD procedures [5]. The reasons of the popularity of ECAP among the SPD methods are the relatively large size of the processable billet and the high degree of homogeneity of the as-received ultrafine-grained (UFG) microstructure [6]. Most of the combined deformation methods consist of ECAP and a subsequent non-SPD procedure, such as plane rolling or extrusion [7]. During rolling, the material is subjected to high hydrostatic stresses, similar to SPD procedures. The combination of ECAP and rolling was applied to different metallic materials, such as titanium [8], copper [9], nickel [10], aluminium alloys [11], magnesium alloys [12], iron and steel [13]. The cold rolling step usually decreases the grain size obtained by the ECAP procedure. Post-rolling not only enhances the strength after ECAP by 20–25%, but also decreases the mechanical heterogeneity throughout the ECAP processed specimen [14]. Significantly higher fraction of high-angle grain boundaries (HAGBs) and larger dislocation density were achieved with the combination of ECAP and rolling than solely with ECAP. The rolling process also yields a transformation of the simple shear texture obtained by ECAP into a rolling texture [13]. The combination of ECAP and rolling can also be applied for the improvement of functional properties of materials. For instance, magnesium processed by ECAP combined with cold rolling yields faster hydrogen absorption kinetics and capacity when compared to the samples deformed only by ECAP. This effect can be explained by the development of a (002) texture which is more favorable for hydrogen absorption and by the formation of a higher amount of defects which act as fast diffusion paths for hydrogen [12].

* Corresponding author.
E-mail address: femkgy@uni-miskolc.hu (G. Krállics).

http://dx.doi.org/10.1016/j.msea.2017.01.112
Received 21 December 2016; Received in revised form 30 January 2017; Accepted 31 January 2017
Available online 01 February 2017

Another important combined deformation method consists of ECAP and traditional extrusion. In the case of extrusion, the deformation state is nearly axisymmetric and a high hydrostatic pressure also acts on the material [15]. It was found that multi-pass warm ECAP combined with cold extrusion considerably improved the mechanical strength of commercially pure Ti due to the significantly reduced grain size [16]. The warm ECAP, as a first step, significantly refined the grain size and increased the yield and ultimate tensile strength values. The second step, cold extrusion, further increased the dislocation density and yielded an elongated grain morphology, which increased both the yield and ultimate tensile strengths by about 50%. When the Ti samples processed by the combined technique were post-annealed at temperatures below 300 °C, the ductility was improved without significant decrease in strength. The major technological limitation of cold extrusion is that the sample needs to be well lubricated before each cold extrusion step to avoid cracking because the friction forces are very high. The combination of ECAP and hydrostatic extrusion also causes improvement of the homogeneity of the microstructure and the mechanical strength, compared to the materials processed only by a single technique [17]. Beside the ECAP-based combined procedures, some other methods can also be used for producing UFG materials. The combination of twist extrusion and hydrostatic extrusion, caliber rolling and drawing, multiple forging and plane rolling are suitable for producing large quantities of UFG materials.

In this paper, the microstructure and the mechanical performance of UFG titanium processed by a combination of multiple forging (MF) and plane rolling are studied. The specimens manufactured by the combined method exhibit high strength and concomitant good ductility. As both processing steps can be easily scaled up for industrial applications, this combined method is capable for mass production of titanium with superior mechanical properties.

2. Experimental and modelling procedures

2.1. Multiple forging and plane rolling

Grade 2 titanium specimens with a length of l_O=100 mm and a square shaped cross section of $a_O \times b_O$=26.5×26.5 mm^2 were used for processing. First, the samples were annealed at 650 °C for 2 h, then they were cooled to room temperature in air. The annealed specimens represent the initial state. The first stage of the combined process was performed by MF under plane strain conditions using a Vacari PV270 friction screw press. The schematic of multiple forging is shown in Fig. 1. Before MF processing the workpiece was heated up to the temperature of 350 °C. Then, the sample was forged in the direction parallel to edge a_O (see Fig. 1a). During this step the dimension a_O=26.5 mm was reduced to a=20 mm while b_O=26.5 mm was increased to b=35 mm, as shown in Fig. 1b. The length l_O=100 mm did not change. In the next step (see Fig. 1c), the workpiece was rotated by an angle of 90° about the axis parallel to l_O and then forged in the direction parallel to edge b. In this step, the prism shape of the specimen with the dimensions of 20×35×100 mm^3 was practically unchanged, as shown in Fig. 1d. This sample was considered as the material processed by one pass of MF. The number of MF passes was increased by repeating the last step of the processing. The first forging step during the first pass of MF is used only for forming the initial square shaped cross section to a rectangular one. After this first step, each MF pass comprises one plane strain deformation step. In this study, the workpieces deformed by 1, 3 and 4 passes were investigated. It should be noted that the temperature of the workpiece decreased from 350 to ~250 °C by the end of the fourth pass of MF, as measured by a probe thermometer.

The samples multiple forged for 4 passes were further deformed by plane rolling. A twin motor rolling mill with the power of 2×7.5 kW was used in the experiments. The diameter of the roll was 180 mm. The speed of rolling was 8 rpm. The rolling direction was parallel to the specimen edge which had a dimension of 35 mm after forging for 4 passes (direction x_3 in Fig. 1). The rolling was performed under three different conditions: (i) the sample was rolled at 20 °C and the thickness was reduced from 20 to 10 mm, (ii) the rolling temperature was 200 °C and the thickness decreased from 20 to 10 mm and (iii) the rolling temperature was 200 °C and the thickness was reduced from 20 to 5 mm. In the cases of (i) and (ii), the dimension of the final product was 10×38×160 mm^3 while for (iii) the sample size was 5×44×270 mm^3. In all cases, the rolling was performed in multiple steps. Above and below the workpiece thickness of 14 mm, the thickness reductions in each rolling step were 2 and 1 mm, respectively.

2.2. Mechanical modelling

Both MF and rolling processes were analysed by a simplified continuum mechanical model using Maple 18 computer algebra software. In the applied model, the material was rigid-plastic. It was assumed for MF that the whole deformation process is homogenous and in plane strain condition (the length of the specimen, l_O, perpendicular to the rolling direction remained unchanged). During MF the Hencky strain tensor (**h**) and the strain rate tensor (**d**) can be written as:

$$\mathbf{h} = \begin{bmatrix} 0 & 0 & 0 \\ 0 & \ln\frac{a}{a_0} & 0 \\ 0 & 0 & -\ln\frac{a}{a_0} \end{bmatrix} \quad \mathbf{d} = \begin{bmatrix} 0 & 0 & 0 \\ 0 & -\frac{v}{a} & 0 \\ 0 & 0 & \frac{v}{a} \end{bmatrix} \tag{1}$$

where a_O and a are the initial and current heights of the workpiece, respectively (see Fig. 1) and v is the velocity of the press ram. The total equivalent strain ($\bar{\varepsilon}$) can be calculated from the equivalent strain rate ($\bar{d}_{eq}$) as:

$$\bar{\varepsilon} = \int_0^t \bar{d}_{eq} dt, \tag{2}$$

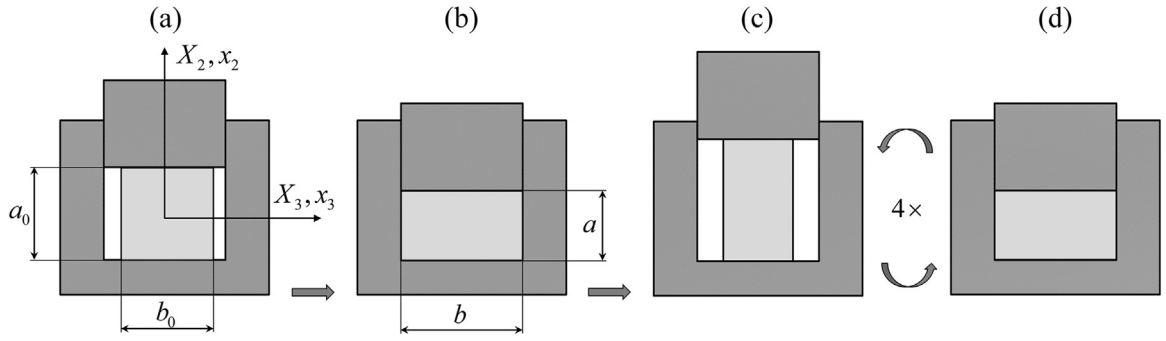

Fig. 1. The sketch of multiple forging. The axes of the coordinate system attached to the sample are denoted as X_1, X_2 and X_3 where axis X_1 is perpendicular to the plane of the figure. The axes of the laboratory coordinate system are denoted as x_1, x_2 and x_3.

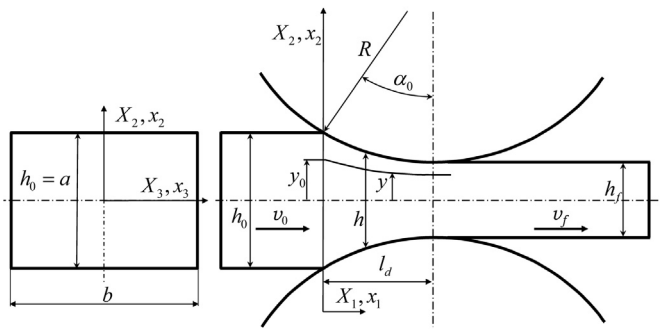

Fig. 2. The sketch of rolling. x_1, x_2, x_3– laboratory coordinates, X_1, X_2, X_3– material coordinates, α_0– angle of bite, h_0, h_f– entry and exit thicknesses, v_0, v_f– entry and exit velocities of the rolled plate, l_d– length of contact zone, R– radius of the roll, y, y_0– a selected streamline and its initial position at the entry of the deformation zone.

where t is the time of processing and $\bar{d}_{eq}$ is obtained from the components of the strain rate tensor using the following formula: $\bar{d}_{eq} = 2/\sqrt{3}(\sqrt{d_{11}^2 + d_{12}^2})$. The thickness reduction during plane rolling occurred in multiple steps. For this manufacturing process, a simplified plane-strain rolling model was applied. The notations used in this calculation are shown in Fig. 2. The initial thickness of the workpiece before rolling was equal to the height achieved in the last (i.e., the fourth) forging step. It is assumed that the planes lying perpendicular to the rolling direction in the initial plate remain planes during rolling. Applying continuity and incompressibility criteria, the components of the velocity vector (v_1, v_2) and the strain rate tensor (d_{11}, d_{22}, d_{12}) can be expressed as:

$$\begin{aligned} &v_1(x_1) = \frac{v_f}{h}h_f, \quad v_2(x_1, x_2) = -\,h_f\frac{v_f}{h^2}h'x_2 \\ &d_{11} = \frac{\partial v_1}{\partial x_1} = -\,h_f\frac{v_f}{h^2}h', \quad d_{22} = \frac{\partial v_2}{\partial x_2} = h_f\frac{v_f}{h^2}h', \quad d_{33} = 0 \\ &d_{12} = \frac{1}{2}\left(\frac{\partial v_1}{\partial x_2} + \frac{\partial v_2}{\partial x_1}\right) = -\,\frac{1}{2}h_f v_f x_2\frac{h''h + 2hh'}{h^4}, \quad d_{13} = d_{23} = 0 \end{aligned} \tag{3}$$

where $h' = \frac{dh}{dx_1}$, $h'' = \frac{d^2h}{dx_1^2}$, and the other quantities are defined in Fig. 2.

The thickness of the rolled plate in the contact zone as a function of coordinate x_1 can be given as:

$$h = h_f + \left(1 - \frac{\sqrt{R^2 - (l_d - x_1)^2}}{R}\right)2R, \tag{4}$$

where $l_d = \sqrt{R\Delta h + (\Delta h/2)^2}$, $\Delta h = h_0 - h_f$. Then, the total equivalent strain can be calculated as:

$$\bar{\varepsilon} = \int_0^t \bar{d}_{eq}dt = \int_{v_1}^{x_1}\frac{\bar{d}_{eq}}{v_1}dx_1 + \Delta\bar{\varepsilon}_I + \bar{\varepsilon}_{prev}, \tag{5}$$

where $\Delta\bar{\varepsilon}_I$ is the strain over the surface discontinuities ($x_1 = 0$, – surface), $\bar{\varepsilon}_{prev}$ is the accumulated strain during the previous deformation. In steady state material flow, the velocity vector components can be expressed by the entry velocity of the rolled plate and the inverse deformation gradient components:

$$v_1 = v_0\frac{\partial X_2}{\partial x_2}, \quad v_2 = -\,v_0\frac{\partial X_2}{\partial x_1}. \tag{6}$$

Using the geometrical assumptions of the present model and the condition of volume constancy, the inverse deformation gradient tensor is obtained as:

$$\mathbf{F}^{-1} = \frac{\partial X_i}{\partial x_k} = \begin{bmatrix} \frac{v_0}{v_1} & 0 & 0 \\ -\frac{v_2}{v_0} & \frac{v_1}{v_0} & 0 \\ 0 & 0 & 1 \end{bmatrix}. \tag{7}$$

The Cauchy deformation tensor can be calculated using the inverse deformation gradient tensor as:

$$\mathbf{c} = \mathbf{F}^{-T}\mathbf{F}^{-1}. \tag{8}$$

Then, the Hencky strain tensor can be determined using the following equation:

$$\mathbf{h} = \mathbf{R}_n(-0.5\ln\boldsymbol{\kappa})\mathbf{R}_n^T \tag{9}$$

where $\mathbf{R}_n$ is the rotation tensor of Eulerian eigen vectors, $\boldsymbol{\kappa}$ is the diagonal tensor from eigen values of Cauchy tensor. Thus, the strain rate and the strain tensors were determined and the mechanical analysis of the manufacturing process was performed.

2.3. Mechanical testing

The mechanical properties of the samples processed by MF and rolling were investigated by uniaxial tensile tests using an Instron universal mechanical testing machine (type 8809) at room temperature and with a cross-head velocity of 6 mm/min. The tests were carried out on cylindrical specimens with the length and diameter of 25 and 5 mm, respectively, machined out from the deformed bars. 3-3 samples were tested for each processing condition (1, 3 and 4 passes of MF, and rolling to 10 mm at 20 °C and 200 °C, and to 5 mm at 200 °C after 4 passes of MF).

2.4. Microstructural examination

The microstructure of the samples processed by MF was studied by an FEI Quanta 3D scanning electron microscope (SEM). The investigated surface for each sample was perpendicular to the compression direction in the last applied MF pass. The surface for electron backscatter diffraction (EBSD) was first mechanically polished with 1200-, 2500- and 4000-grit SiC abrasive papers. Then, the polished surface was ion milled by an Ar-ion beam using SEMPrep2 device (manufacturer: Technoorg Linda Ltd., Budapest, Hungary). During ion milling, the samples were cooled to liquid nitrogen temperature in order to avoid unwanted annealing. The EBSD images were taken with the step size of 30 nm and evaluated by OIM software made by TexSem Laboratories.

The grain structures in the initial and the rolled specimens were examined by a Tecnai G2 X-TWIN transmission electron microscope (TEM). In the case of the rolled specimens, the TEM foils were prepared from the longitudinal sections containing the rolling and the normal directions which were thinned by mechanical grinding to a thickness of 20–40 μm. Then, the foils were further thinned by Ar-ion milling using a Gatan Model 691 precision ion polishing system. Automated Crystallographic Orientation Mapping (ACOM) was also performed in TEM using ASTAR technique.

The microstructures of the initial specimen and the samples processed by MF and rolling were also examined by X-ray line profile analysis (XLPA). For the samples processed by MF, the XLPA investigations were carried out on the surface lying normal to the last forging direction. In the case of the rolled specimens, the XLPA study was performed on the surface containing the rolling and the normal directions (the same surface as that one studied by TEM). It is noted that the diffraction peak breadths were practically the same for other surfaces. Before XLPA measurements, the surface was mechanically polished to a mirror finish with a diamond paste. Then, the surface layer distorted during polishing was removed by chemical etching using hydrogen fluoride. The X-ray line profiles were measured by a high-resolution rotating anode diffractometer (Rigaku, RA Multimax9) using CuKα_1 (λ=0.15406 nm) radiation. Two-dimensional imaging plates were used for the detection of the Debye–Scherrer diffraction rings. The line profiles were determined by integrating the two dimensional intensity distribution along the rings. The X-ray diffraction patterns were evaluated by the Convolutional Multiple Whole Profile (CMWP) fitting method [18]. In this procedure, the diffraction pattern is fitted by the sum of a background spline and the convolution

of the instrumental pattern and the theoretical line profiles related to the crystallite size and dislocations. The instrumental pattern was measured on a LaB_6 line profile standard material. The CMWP evaluation program selects automatically the nearest instrumental profile to each diffraction peak of the samples. It is noted that the instrumental broadening was about 4–10 times smaller than the breadth of the diffraction profiles for the severely deformed Ti samples investigated in this study. Therefore, the instrumental correction had only a marginal effect on the microstructural parameters determined by XLPA method. The theoretical profile functions used in the fitting procedure were calculated on the basis of a model of the microstructure, where the crystallites have spherical shape and log-normal size distribution, and the lattice strains are caused by dislocations. Twenty-one peaks of Ti were fitted in the evaluation of line profiles. The area-weighted mean crystallite size ($< x >_{area}$) and the dislocation density (ρ) were obtained from this method. The CMWP procedure also enables the determination of the prevailing dislocation slip systems in hexagonal crystals. The experimental values of parameters q_1 and q_2 in the dislocation contrast factors obtained by the CMWP method depend on the type of dislocations. The theoretical q_1 and q_2 values for the eleven possible slip systems in Ti have been calculated according to Kuzel and Klimanek [19] and listed in Table 2 in Ref. [20]. The eleven dislocation slip systems can be classified into three groups based on their Burgers vectors: $b_1 = 1/3\langle\bar{2}110\rangle$ ($< a >$ type), $b_2 = \langle 0001\rangle$ ($< c >$ type) and $b_3 = 1/3\langle\bar{2}113\rangle$ ($< c+a >$ type). The comparison between the experimental and theoretical values of parameters q_1 and q_2 yields the fractions of the different types of dislocations [21].

3. Results

3.1. Mechanical behavior of MF-processed and rolled Ti samples

The mechanical properties of the initial material and the samples deformed by MF and rolling are shown in Fig. 3. The values of the yield strength, ultimate tensile strength, elongation to failure, reduction in area and strain energy density to fracture were obtained as the average of four measurements. The yield and ultimate tensile strength values of the initial material were 332 and 439 MPa, respectively. MF processing at 350 °C yielded a significant improvement in both strength values. After 4 passes of MF, the yield and the ultimate tensile strength values increased to 445 and 620 MPa, respectively. The parameters describing the ductility of materials, i.e., the elongation to failure and the reduction in area did not change considerably due to MF processing.

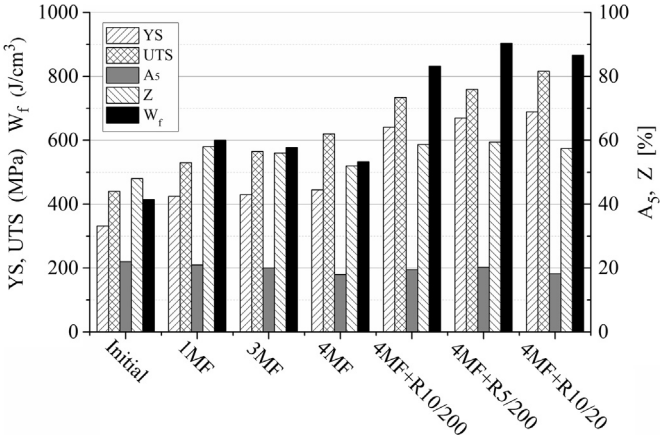

Fig. 3. Mechanical properties of Grade 2 titanium in the initial, multiple forged and rolled states. YS - yield strength, UTS - ultimate tensile strength, A5 -elongation to failure, Z - reduction in area, W_f - strain energy density to fracture. The samples are denoted as: 1MF, 3MF and 4MF – MF processing for 1, 2 and 4 passes, respectively; 4MF + R10/200 and 4MF + R5/200 – rolling at 200 °C to the thickness of 10 and 5 mm, respectively, after 4 passes of MF; 4MF + R10/20 – rolling at 20 °C to the thickness of 10 mm after 4 passes of MF.

For the sample deformed by four MF passes, the elongation to failure was 18% while the reduction in area was 52%. Fig. 3 shows that MF processing yielded an increase in the strain energy density to fracture from 414 to 533 J/cm^3, which is mainly caused by the rise of strength.

Rolling after four passes of MF resulted in an additional improvement in strength, as shown in Fig. 3. When the samples were rolled at 200 °C to the thickness values of 10 and 5 mm, the yield strength increased to 641 and 669 MPa, respectively. The ultimate tensile strength values were 734 and 759 MPa for these materials. The highest yield and ultimate tensile strength values achieved by rolling at 20 °C to the thickness of 10 mm were 689 and 816 MPa, respectively. Concomitantly with the increase of strength, the ductility did not deteriorate considerably. After rolling at 20 °C, the elongation to failure and the reduction in area were 18% and 57%, respectively. Due to the practically unchanged elongation to failure and the very high strength increment, rolling at 20 °C yielded much higher strain energy density to fracture (866 J/cm^3) than that in the initial state (414 J/cm^3).

3.2. Microstructure of the MF-processed and rolled samples

The crystallite size, the density and the fractions of $< a >$, $< c >$ and $< c+a >$ dislocations were determined by XLPA. Fig. 4 shows the CMWP fitting for the sample rolled at 200 °C to the thickness of 10 mm. The microstructural parameters obtained by XLPA are shown in Table 1. It can be seen that the crystallite size is small (~72 nm) while the dislocation density is large (~9×10^{14} m^{-2}) even after the first pass of MF which changed only slightly with increasing the number of MF passes up to four. Subsequent rolling yielded only a negligible reduction of the crystallite size. At the same time, the dislocation density increased to ~18×10^{14} m^{-2} due to rolling at 200 °C to the thickness of 10 mm. The larger thickness reduction to 5 mm did not yield smaller crystallite size or higher dislocation density. This observation suggests that in the rolling process at 200 °C a saturation of the microstructure was achieved already at the thickness reduction to 10 mm, therefore more severe rolling did not yield further increment in the dislocation density. In addition, the decrease of the rolling temperature to 20 °C also did not lead to a higher dislocation density. This result can be explained by the fact that the sample rolled nominally at 20 °C also underwent a warm deformation since the temperature of the workpiece increased by about 100–150 °C during rolling, owing to the friction between the rolls and the material, as well as the transformation of plastic work into heat. Therefore, the dislocation density values were similar in the samples rolled at 200 and 20 °C.

The fractions of $< a >$, $< c >$ and $< c+a >$ dislocations were also determined for the samples processed by MF and subsequent rolling.

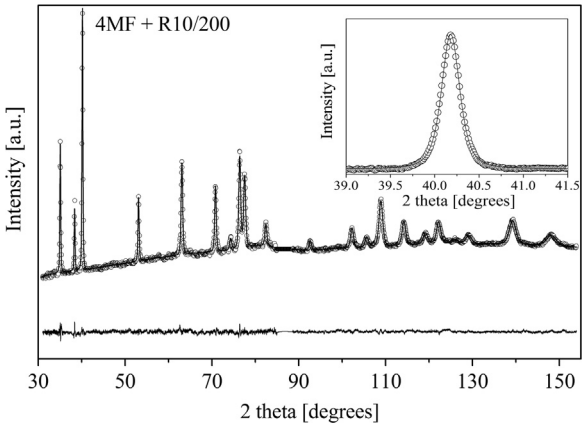

Fig. 4. The measured (open circles) and the fitted theoretical (solid line) X-ray diffraction patterns obtained on the sample rolled to a thickness of 10 mm at 200 °C (denoted as 4MF + R10/200). The difference between the measured and the fitted patterns is shown at the bottom of the figure. The inset shows peak *101* with higher magnification.

Table 1
Parameters of the microstructure obtained for the initial specimen and the samples processed by MF and rolling. The notations of the samples are given in the caption of Fig. 1.

Sample	Grain size [μm]	Crystallite size [nm]	Dislocation density [10^{14} m^{-2}]
Initial	20	> 1000	< 0.1
1MF	2	72 ± 8	9 ± 1
3MF	–	67 ± 7	9 ± 1
4MF	1.5	71 ± 7	11 ± 1
4MF+R10/200	0.89	63 ± 6	18 ± 2
4MF+R5/200	0.87	60 ± 6	17 ± 2
4MF+R10/20	0.56	58 ± 7	18 ± 2

For all materials the $<a>$ dislocations have the highest fraction (72–78%), while the fraction of $<c+a>$ dislocations is only 18–26%. The amount of $<c>$ dislocations is negligible. The abundance of $<a>$-type dislocations can be attributed to their lowest energy due to the smallest Burgers vector. It was also revealed that among $<a>$-type dislocations the fraction of prismatic edge dislocations is much higher than those for basal or pyramidal dislocations. This can be explained by the easier slip of prismatic dislocations than the other ones which is a common feature of hexagonal structures with the ratio of lattice parameters lower than 1.63 [22]. In the $<c+a>$ dislocation group, the pyramidal edge dislocations with the Burgers vectors of $\frac{1}{3}\langle\bar{2}113\rangle\{2\bar{1}\bar{1}2\}$ and $\frac{1}{3}\langle\bar{2}113\rangle\{10\bar{1}1\}$ have the highest fractions.

Fig. 5 shows EBSD images of the microstructures for the samples processed by one and four passes of MF (i.e., for the lowest and highest strains applied in MF processing). The grains are defined as the volumes bounded by boundaries with misorientation angles larger than 15°. The grain size of the initial annealed material was about 20 μm [23]. The EBSD images in Fig. 5 reveal that the grain size decreased to 2 and 1.5 μm after one and four passes of MF at 350 °C, respectively. The average grain size values are also listed in Table 1. It can also be seen in Fig. 5 that the grain size distribution is broad, consisting of both large and small grains.

The ACOM-TEM images in Fig. 6 illustrate the microstructures of the samples rolled after four MF passes. The average grain sizes determined from the TEM images are listed in Table 1. It can be seen that rolling resulted in an additional grain refinement, compared to the sample processed by four MF passes. The rolling at 200 and 20 °C

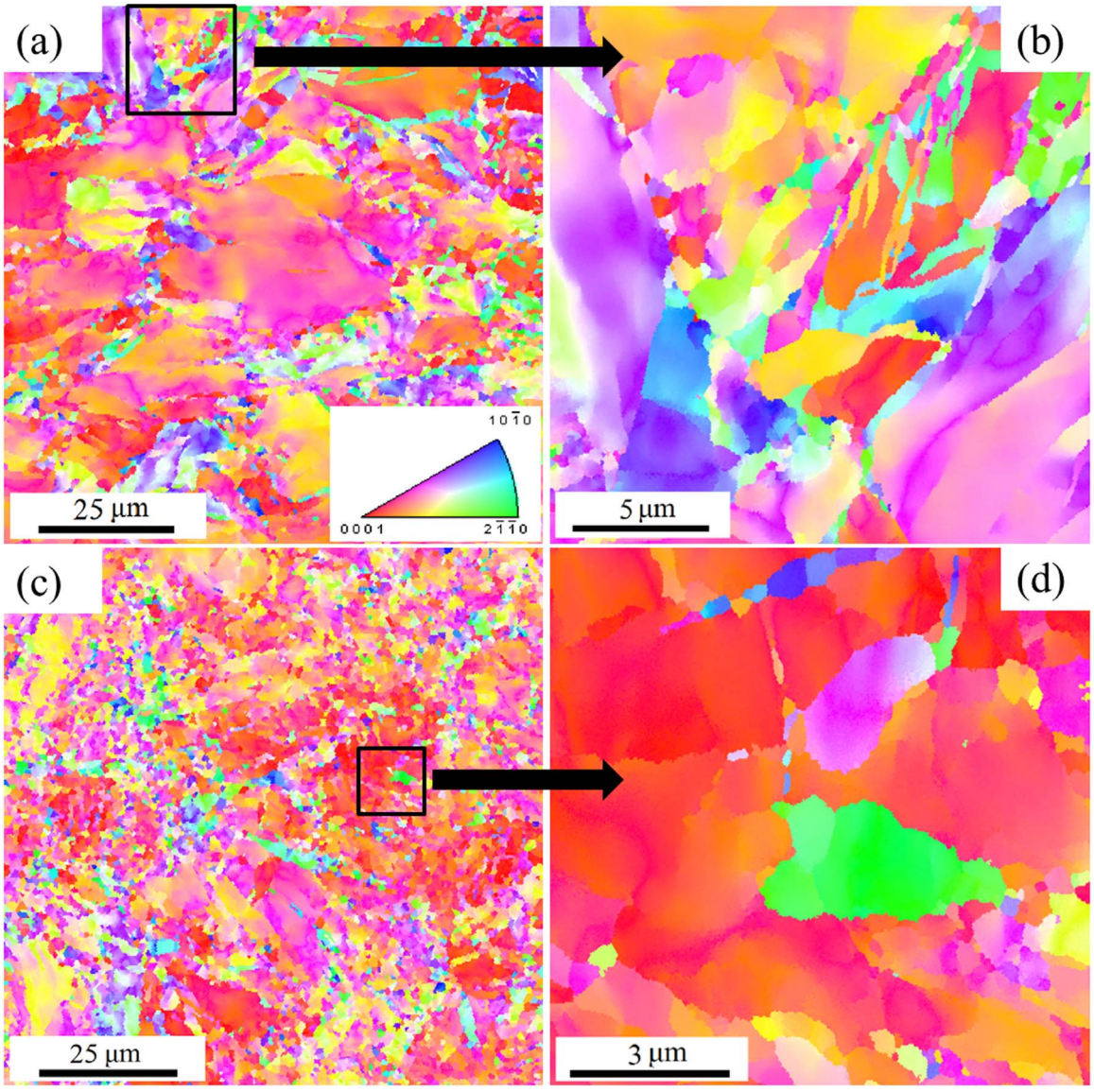

Fig. 5. EBSD images showing the microstructures of the samples processed by one pass (a,b) and four passes (c,d) of MF. Figures (b) and (d) show magnified parts of figures (a) and (c), respectively.

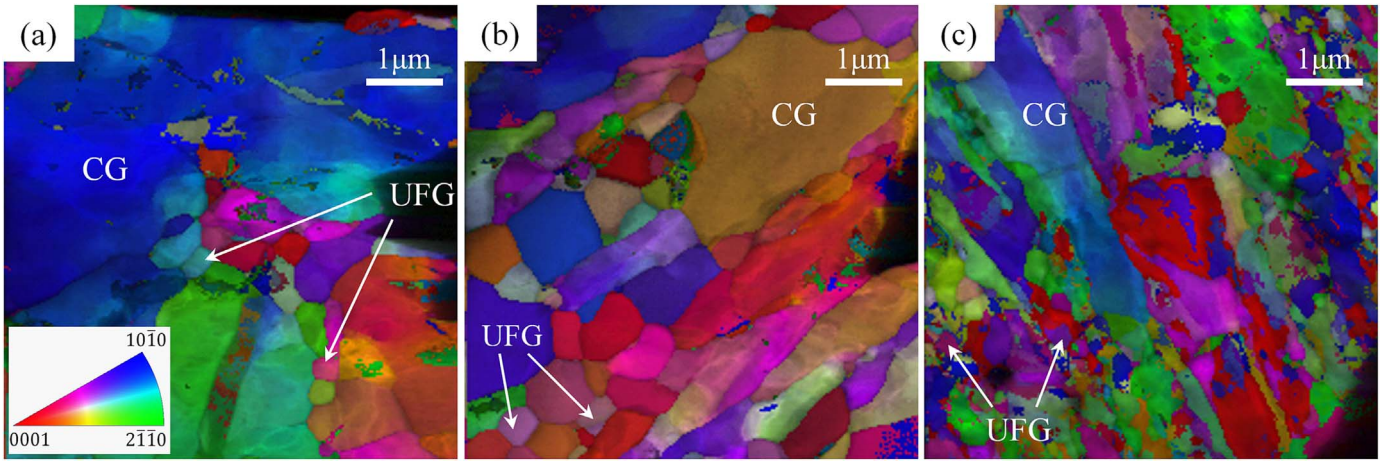

Fig. 6. TEM images showing the microstructures of the samples rolled to (a) a thickness of 10 mm at 200 °C, (b) a thickness of 5 mm at 200 °C and (c) a thickness of 10 mm at 20 °C. The abbreviations CG and UFG indicate coarse and ultrafine grains, respectively.

yielded to a reduction of the average grain size from about 1.5 μm to 870–890 and 560 nm, respectively. It seems that in the rolling process at 200 °C the saturation grain size was achieved even after the thickness reduction to 10 mm, as further straining to the thickness of 5 mm did not lead to further considerable grain refinement. At the same time, the decrease of the rolling temperature to 20 °C yielded smaller grain size. It can be concluded that UFG microstructures were achieved by the combination of MF and rolling processes.

3.3. Mechanical analysis of MF and rolling processes

The components of the strain rate tensor, the equivalent strain rate and the total equivalent strain were calculated as a function of time for the whole MF process and plotted in Fig. 7a. At the end of MF processing, the total equivalent strain reaches about 2.3. The components of the Hencky strain tensor and the equivalent Hencky strain versus time are shown for the MF process in Fig. 7b. The common characteristic of the SPD processes is the non-monotonic nature of the deformation. The concept of monotonic deformation was introduced by Smirnov-Aljajev [24]. As he wrote, a forming process develops monotonically if no component of the strain rate tensor changes its sign, i.e., the eigenvectors of the strain rate tensor are parallel to the eigenvectors of the strain tensor during the whole deformation process and the Lode parameter remains constant. The strain path change (SPC) parameter, developed by Schmitt et al. [25] is a quantity which characterizes the change of the deformation history, using the deformation tensor in different instants of time. Using the Hencky strain (**h**) and strain rate (**d**) tensors at the same time, the modified strain path change parameter (SPC_{mod}) can be given as:

$$SPC_{\mathrm{mod}} = \frac{(\mathbf{h}:\mathbf{d})}{(\mathbf{h}:\mathbf{h})^{\frac{1}{2}}(\mathbf{d}:\mathbf{d})^{\frac{1}{2}}}. \tag{10}$$

The variation of parameter SPC_{mod} as a function of processing time in MF deformation is shown in Fig. 7b. The second part of the combined forming process is the rolling. The results of the mechanical calculation for rolling are presented in Figs. 8 and 9. From the SPC_{mod} versus time plot it is clear that the MF process has cyclic non-monotonic character and at the end of the MF process the total equivalent strain is more than two. Therefore, four passes of MF yields similar equivalent strain as two passes of ECAP, i.e., it is capable to produce fine-grained microstructure. Figs. 8 and 9 reveal that the rolling process is nearly monotonic and at the end of the rolling process the total equivalent strain reaches 4.35. The high strain value at the end of the combined process explains the UFG microstructure and the related high strength observed in Ti. At the same time, contrary to the laboratory SPD-processes such as ECAP, the processes of MF and rolling can be easily applied in industrial environments.

4. Discussion

The present study demonstrates that the combined deformation process including MF and subsequent rolling resulted in a titanium

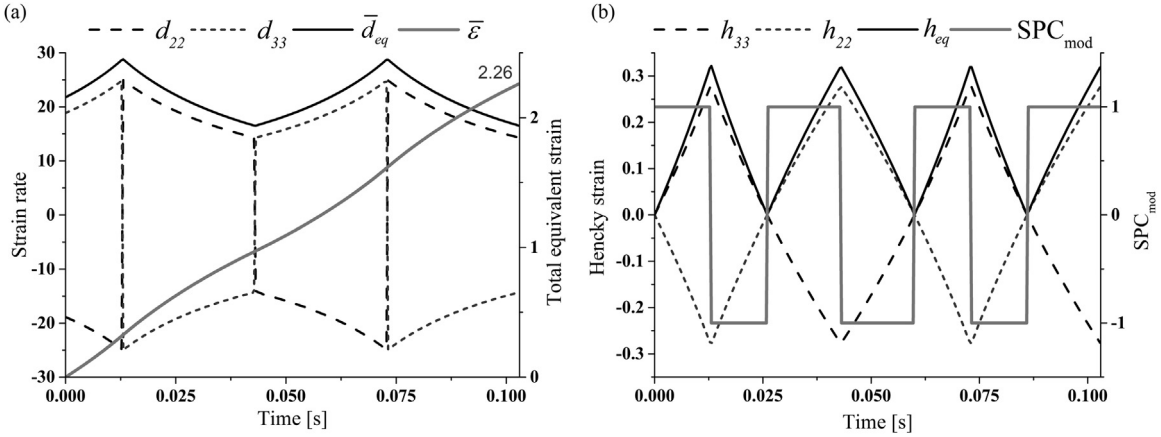

Fig. 7. (a) The non-zero components of the strain rate tensor (d_{22} and d_{33}), the equivalent strain rate ($\bar{d}_{eq}$) and the total equivalent strain ($\bar{\varepsilon}$), as well as (b) the non-zero components of the Hencky strain tensor (h_{22} and h_{33}), the Hencky strain (h_{eq}) and the modified strain path change parameter (SPC_{mod}) as a function of time for the MF process. The results are obtained by a simplified continuum mechanical model (see Section 2.2).

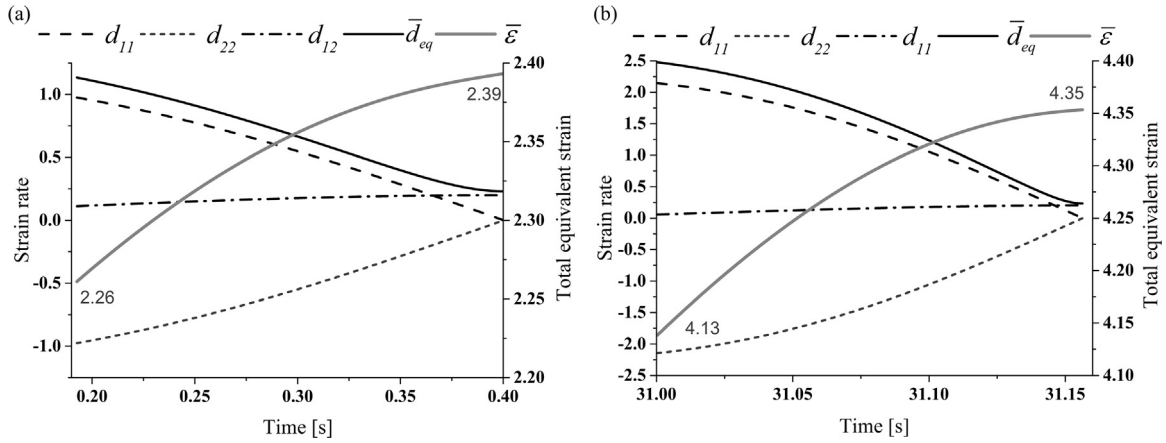

Fig. 8. The non-zero components of the strain rate tensor (d_{11}, d_{22} and d_{12}), the equivalent strain rate ($\bar{d}_{eq}$) and the total equivalent strain ($\bar{\varepsilon}$) as a function of time in the (a) first and (b) last passes of rolling. The results are obtained by a simplified continuum mechanical model (see Section 2.2).

with high strength and good ductility. The enhanced strength can be attributed to the high dislocation density and the UFG microstructure. It should noted, however, that the dislocation density achieved by the combination of MF and rolling processes (~18×10^{14} m^{-2}) was somewhat smaller than the value achieved by the combination of warm ECAP at 450 °C and cold rolling in a former work (~30×10^{14} m^{-2}, [26]). Most probably, in the previous study the lower temperature of rolling was the reason of the higher value of the dislocation density. Accordingly, the yield strength values of the present rolled materials (641–689 MPa) were smaller than the corresponding value for the ECAP processed and cold rolled titanium (~900 MPa, [26]). At the same time, the forging and rolling techniques used in this study are more productive than ECAP and they can be applied in industrial environments.

The combination of MF and rolling resulted in a decrease of the average grain size into the UFG regime, as shown in Table 1. However, the TEM images in Fig. 6 suggest that the grain size distributions in all rolled specimens have a bimodal character. Indeed, beside the utrafine grains (smaller than 1 μm) coarse grains can also be observed in Fig. 6 (denoted as CG). These coarse grains may be formed due to the elevated temperature of deformation. It should be noted here that the sample rolled nominally at 20 °C also underwent warm deformation due to the increase of the workpiece temperature during rolling, as discussed in Section 3. The high temperature during rolling facilitates dynamic recovery and recrystallization which result in grain growth. As the temperature of deformation is not very high compared to the melting point, only a partial recovery/recrystallization occurred, resulting in the formation of embedded coarse grains in the UFG matrix. Most probably, this bimodal microstructure is a crucial factor in the achievement of the improved mechanical properties with high strength and good ductility. It is worth to note that during MF and rolling performed at high temperatures simultaneous grain refinement and dynamic recovery/recrystallization occurred, therefore the dislocation density only slightly changed with increasing the imposed strain.

In a recently published work on Ti [27], it was also shown that a heterogeneous lamella structure with coarse and UFG volumes exhibited superior mechanical behavior: the material was as hard as an UFG microstructure and at the same time as ductile as a conventional coarse-grained Ti. In that study, the inhomogeneous microstructure was achieved by asymmetric rolling with a thickness reduction of 87.5% and a subsequent annealing at 475 °C for 5 min which resulted in a partial recrystallization of the severely deformed material. The significance of the present study is that this heterogeneous microstructure with superior mechanical performance can also be achieved by a combined process of MF and rolling, without additional annealing. As these processes can easily be transposed into an industrial environment, therefore the combined method may be a candidate technique for mass production of Ti with high strength and good ductility.

5. Conclusions

UFG-Ti with Grade 2 purity was processed by a combination of MF and plane rolling. The evolution of the microstructure and the mechanical properties were monitored after each step of this technol-

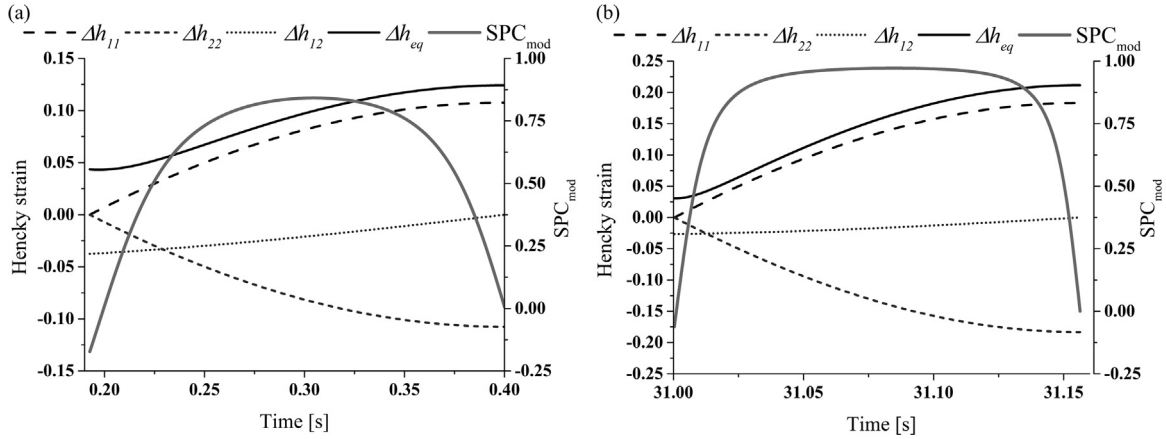

Fig. 9. The change of the non-zero components of the Hencky tensor (Δh_{11}, Δh_{22} and Δh_{12}) and the change of the Hencky strain (Δh_{eq}) as a function of time during the (a) first and (b) last passes of rolling. The evolution of the modified strain path change parameter (SPC_{mod}) is also shown. The results are obtained by a simplified continuum mechanical model (see Section 2.2).

ogy. In addition, the deformation processes were analysed by a simplified continuum mechanical model. From the results the following conclusions can be drawn:

1. The grain size decreased from ~20 μm to ~1.5 μm while the dislocation density increased to ~11×10^{14} m^{-2} due to 4 passes of MF at 350 °C. Accordingly, the yield strength significantly increased from 332 to 439 MPa and the ultimate tensile strength rose from 445 to 620 MPa. Concomitantly, only a marginal reduction of the elongation to failure was observed (from 22% to 18%).
2. Additional plane rolling at room temperature after 4 passes of MF yielded further grain refinement to ~560 nm while the dislocation density increased to ~18×10^{14} m^{-2}. Rolling at elevated temperature (200 °C) resulted in a higher grain size (about 870 nm). The fine grain size and the high dislocation density obtained by the combined process led to very high yield and tensile strength values of 689 and 816 MPa, respectively. At the same time, considerable reduction of ductility was not observed since the elongation to failure remained ~18%. Therefore, it was shown that the combination of MF and plane rolling yielded an UFG microstructure in Grade 2 titanium which exhibits both high strength and good ductility. The very good ductility can be attributed to the coarse grains embedded in the UFG matrix which are formed most probably due to a dynamic recovery and/or recrystallization during deformation.
3. Mechanical modelling of the combined process revealed a large equivalent strain, which is an important condition for effective grain refinement. The non-monotonic nature of MF process was also shown which might also contribute to the evolution of the UFG microstructure.
4. The MF step of the proposed combined manufacturing method was carried out in an industrial environment. Therefore, this technology might be a candidate process for mass-production of UFG titanium with high strength and good ductility.

Acknowledgements

This research was supported by the Hungarian Scientific Research Fund (OTKA), Grant nos. K119566 and K109021. The surface of the Ti samples processed by MF were prepared for EBSD using SEMPrep2 device (manufacturer: Technoorg Linda Ltd., Budapest, Hungary). The authors are grateful to Ms. Nóra Nagy and Dr. Károly Havancsák for the surface preparation of the EBSD specimens.

References

[1] T.G. Langdon, Twenty-five years of ultrafine-grained materials: achieving exceptional properties through grain refinement, Acta Mater. 61 (2013) 7035–7059.
[2] J. Gubicza, N.Q. Chinh, J.L. Lábár, S. Dobatkin, Z. Hegedus, T.G. Langdon, Correlation between microstructure and mechanical properties of severely deformed metals, J. Alloy. Compd. 483 (2009) 271–274.
[3] Y. Estrin, A.V. Vinogradov, Extreme grain refinement by severe plastic deformation: a wealth of challenging science, Acta Mater. 61 (2013) 782–817.
[4] Y. Iwahashi, Z. Horita, M. Nemoto, T.G. Langdon, An investigation of microstructural evolution during equal-channel angular pressing, Acta Mater. 45 (1998) 4733–4741.
[5] M. Kulczyk, J. Skiba, W. Pachla, Microstructure and mechanical properties of AA5483 treated by a combination of ECAP and hydrostatic extrusion, Arch. Metall. Mater. 59 (2014) 163–166.
[6] R.Z. Valiev, T.G. Langdon, Principles of equal-channel angular pressing as a processing tool for grain refinement, Prog. Mater. Sci. 51 (2006) 881–981.
[7] D. Nagarajan, U. Chakkingal, P. Venugopal, Influence of cold extrusion on the microstructure and mechanical properties of an aluminium alloy previously subjected to equal channel angular pressing, J. Mater. Process. Technol. 182 (2007) 363–368.
[8] V.V. Stolyarov, Y.T. Zhu, I.V. Alexandrov, T.C. Lowe, R.Z. Valiev, Grain refinement and properties of pure Ti processed by warm ECAP and cold rolling, Mater. Sci. Eng. A 343 (2003) 43–50.
[9] N.D. Stepanova, A.V. Kuznetsova, G.A. Salishcheva, G.I. Raab, R.Z. Valiev, Effect of cold rolling on microstructure and mechanical properties of copper subjected to ECAP with various numbers of passes, Mater. Sci. Eng. A 554 (2012) 105–115.
[10] N.A. Krasilnikov, W. Lojkowski, Z. Pakiela, K.J. Kurzydlowski, Mechanical properties and deformation behaviour of ultra-fineultra-fine grained nickel, Solid State Phenom. 114 (2006) 79–84.
[11] K.T. Park, H.J. Lee, C.S. Lee, W.J. Nam, D.H. Shin, Enhancement of high strain rate superplastic elongation of a modified 5154 Al by subsequent rolling after equal channel angular pressing, Scr. Mater. 51 (2004) 479–483.
[12] G.F. Lima, M.R.M. Triques, C.S. Kiminami, W.J. Botta, A.M. Jorge, Hydrogen storage properties of pure Mg after the combined processes of ECAP and cold rolling, J. Alloy. Compd. 586 (2014) 405–408.
[13] L. Wu, J. Chen, Z. Du, J. Wang, Microstructures of ultra-fine grained FeCoV alloys processed by ECAP plus cold rolling and their evolutions during tempering, Trans. Nonferr. Met. Soc. 20 (2010) 602–606.
[14] S.R. Bahadori, K. Dehghani, F. Bakhshandeh, Microstructure, texture and mechanical properties of pure copper processed by ECAP and subsequent cold rolling, Mater. Sci. Eng. A 583 (2013) 36–42.
[15] D.H. Kang, T.W. Kim, Mechanical behavior and microstructural evolution of commercially pure titanium in enhanced multi-pass equal channel angular pressing and cold extrusion, Mater. Des. 31 (2010) 54–60.
[16] V.V. Stolyarov, Y.T. Zhu, T.C. Lowe, R.Z. Valiev, Microstructure and properties of pure Ti processed by ECAP and cold extrusion, Mater. Sci. Eng. A 303 (2001) 82–89.
[17] M. Kulczyk, W. Pachla, A. Mazur, M. Sus-Ryszkowska, N. Krasilnikov, K.J. Kurzydlowski, Producing bulk nanocrystalline materials by combined hydrostatic extrusion and equal-channel angular pressing, Mater. Sci. Pol. 25 (2007) 992–999.
[18] G. Ribárik, J. Gubicza, T. Ungár, Correlation between strength and microstructure of ball milled Al-Mg alloys determined by X-ray diffraction, Mater. Sci. Eng. A 387–389 (2004) 343–347.
[19] R. Kuzel Jnr, P. Klimanek, X-ray diffraction line broadening due to dislocations in non-cubic crystalline materials. III. Experimental results for plastically deformed zirconium, J. Appl. Crystallogr. 22 (1989) 299–307.
[20] I.C. Dragomir, T. Ungár, Contrast factors of dislocations in the hexagonal crystal system, J. Appl. Crystallogr. 35 (2002) 556–564.
[21] J. Gubicza, X-ray Line Profile Analysis in Materials Science, IGI-Global, Hershey, PA, USA, 2014.
[22] H.J. Frost, M.F. Ashby, Deformation-Mechanism Maps: The Plasticity and Creep of Metals and Ceramics, Pergamon Press, Oxford, UK, 1982.
[23] J. Gubicza, Zs Fogarassy, Gy Krállics, J. Lábár, T. Törköly, Microstructure and mechanical behavior of ultrafine-grained titanium, Mater. Sci. Forum 589 (2008) 99–104.
[24] G.A. Smirnov-Aljajev, Soprotivlenije materialov plasticheshkomu deformirovaniju, Masinostroenije, Leningrad, SSSR, 1978.
[25] J.H. Schmitt, E.L. Shen, J.L. Raphanel, A parameter for measuring the magnitude of a change of strain path: validation and comparison with experiments on low carbon steel, Int. J. Plast. 10 (1994) 535–551.
[26] Y.T. Zhu, J.Y. Huang, J. Gubicza, T. Ungár, Y.M. Wang, E. Ma, R.Z. Valiev, Nanostructures in Ti processed by severe plastic deformation, J. Mater. Res. 18 (2003) 1908–1917.
[27] X. Wu, M. Yang, F. Yuan, G. Wu, Y. Wei, X. Huang, Y. Zhu, Heterogeneous lamella structure unites ultrafine-grain strength with coarse-grain ductility, Proc. Natl. Acad. Sci. USA 112 (47) (2015) 14501–14505.